Supramolecular heptanuclear Ln–Cu complexes involving nitronyl nitroxide biradicals: structure and magnetic behavior

Lu Xi, Chao-Yi Jin, Hong-Wei Song, Xiao-Tong Wang, Li-Cun Li, J. P. Sutter

Supramolecular heptanuclear Ln-Cu complexes involving nitronyl nitroxide biradicals: structure and magnetic behavior

Lu Xi,[a] Chao-Yi Jin,[a] Hong-Wei Song,[a] Xiao-Tong Wang,[a] Li-Cun Li*[a] and Jean-Pascal Sutter*[b]

[a] *Department of Chemistry, Key Laboratory of Advanced Energy Materials Chemistry, College of Chemistry, Nankai University, Tianjin 300071, China*

[b] *Laboratoire de Chimie de Coordination du CNRS (LCC-CNRS), Université de Toulouse, CNRS, Toulouse, France*

** Corresponding author E-mail address:*

llicun@nankai.edu.cn

jean-pascal.sutter@lcc-toulouse.fr

Abstract

Four novel heptanuclear Ln–Cu complexes with formula $[Ln_2Cu(hfac)_8(NITPhTzbis)_2][LnCu(hfac)_5(NITPhTzbis)]_2$ (LnCu = YCu **1**, TbCu **2**, DyCu **3** and HoCu **4**; hfac = hexafluoroacetylacetonate) were successfully constructed by employing the triazole functionalized nitronyl nitroxide biradical ligand NITPh-Tzbis (NITPh-Tzbis = 5-(1,2,4-triazolyl)-1,3-bis(1′-oxyl-3′-oxido-4′,4′,5′,5′-tetramethyl-4,5-hydro-1*H*-imidazol-2-yl)benzene). These hetero-tri-spin complexes are composed of two biradical-bridged dinuclear $[(LnCu(hfac)_5(NITPhTzbis)]$ units and one trinuclear $[Ln_2Cu(hfac)_8(NITPhTzbis)_2]$ unit which form a heptanuclear supramolecular structure through π–π interactions. Magnetic susceptibility investigations indicate that ferromagnetic exchange interactions dominate at low temperature for this supramolecular system which can be attributed to the Ln-nitroxide exchange and intramolecular NIT---NIT coupling mediated by the *m*-phenylene moiety. The DyCu derivative was found to exhibit slow magnetic relaxation behavior.

Introduction

The development of single-molecule magnets (SMMs) containing Ln ions has been one of the frontiers of research in the field of SMMs since the turn of the century[1-5] owing to the strong magnetic anisotropy and the large magnetic moments of the lanthanides ions. Employing this approach, some remarkable achievements have been obtained,[6-9] such as the $[(Cp^{iPr5})Dy(Cp^{*})]^{+}$ complex with a record anisotropic energy barrier of 2217 K and a blocking temperature of 80 K, which is the best SMM reported to date.[10] However, some challenges remain to be mastered, like quantum tunneling of magnetization (QTM) caused by inherent characteristic of lanthanide ions, which brings about a rapid decay of magnetization at zero field. A promising approach is to implement a large exchange interaction with the rare earth centers in poly-spin complexes.[11-17] Nevertheless, achieving a strong exchange interaction with Ln ions is not obvious because the 4f magnetic orbitals are shielded by the more external 5s and 5p electron clouds. In this context, the use of paramagnetic radical ligands is an attractive strategy in which the direct exchange between lanthanide ion and coordinated radical could be achieved.[18] In 2011, Long *et al*[19] reported a N_2^{3-} radical bridged Tb_2 complex exhibiting blocking temperature of 14 K, which demonstrated that better SMM properties can be achieved by introducing organic radicals in the Ln-based complexes. Murugesu *et al*[20] successfully obtained a Dy_4 complex by employing highly delocalized tetrazinyl radicals, which result a magnet-like behaviour with a large coercive field of 30 kOe in this complex. Most extreme situation, reported by Popov's group,[21] is found in dimetallofullerene compounds featuring a covalent lanthanide-lanthanide bond containing an unpaired electron acting as paramagnetic bridge between the Ln centers. These compounds exhibited remarkable magnetic relaxation behavior , as illustrated by $Tb_2@C_{80}(CH_2Ph)$ with a blocking temperature near 30 K.[22]

Nitronyl nitroxide radicals (NIT), owing to their stability and ease of chemical modification,[23, 24] have been widely used for the construction of molecular nanomagnets.[25-30] While most attention focused on mono-nitronyl nitroxide radicals, poly-radical ligands provide new opportunities to obtain diverse spin topologies and interesting magnetic properties.[31-33] On the other hand, combining 3d ions and 4f ions within a molecular entity by the means of radical ligands has

emerged as a promising approach for designing molecular magnetic materials in which the magnetic exchanges and the ligand field could be finely tuned.[34-39]

Herein, a novel nitronyl nitroxide biradical ligand with a triazole group, *i.e*. NITPhTzbis (5-(1,2,4-triazolyl)-1,3-bis(1′-oxyl-3′-oxido-4′,4′,5′,5′-tetramethyl-4,5-hydro-1*H*-imidazol-2-yl) benzene, Scheme 1) was employed to construct new biradical-4f-3d systems. Accordingly, four biradical heterometallic complexes $[Ln_2Cu(hfac)_8(NITPhTzbis)_2][LnCu(hfac)_5(NITPhTzbis)]_2$ (LnCu = YCu **1**, TbCu **2**, DyCu **3**, HoCu **4**; hfac = hexafluoroacetylacetonate) were obtained. These 2*p*-3*d*-4*f* complexes present a heptanuclear supramolecular structure consisting of two dinuclear units $[LnCu(hfac)_5(NITPhTzbis)]$ and one trinuclear unit $[Ln_2Cu(hfac)_8(NITPhTzbis)_2]$. Magnetic studies revealed that the ferromagnetic couplings are predominant in these complexes. Slow magnetic relaxation behavior was observed for DyCu derivative.

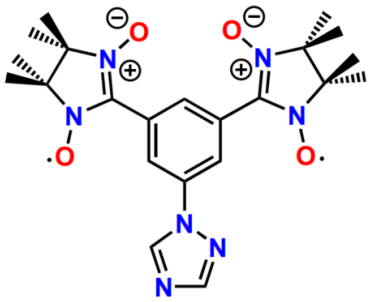

Scheme 1. NITPhTzbis radical ligand.

Experimental

Materials and physical measurements.

All solvents and other reagents (AR grade) for the experiments were commercially available and used as received without any further purification, and nitronyl nitroxide biradical NITPhTzbis was prepared according to literature procedure.[40, 41] Elemental analysis was performed by a Perkin-Elmer 240 elemental analyzer. FT-IR data were tested using a Bruker-Vector 22 Spectrophotometer. Powder X-ray diffraction (PXRD) data of the as-prepared **1**–**4** was obtained on a Rigaku Ultima IV diffractometer at room temperature. Magnetic data were obtained on a Quantum Design MPMS 5S SQUID magnetometer and a PPMS-9 magnetometer. The magnetic measurements were performed on crystalline powder samples mixed with grease and hold in a

gelatin capsule. The diamagnetic corrections for direct-current data were made for the constituent atoms using Pascal's constants.[42] The crystalline phase purities of four complexes are confirmed by PXRD (Figure S1).

Crystallography.

The structures of **1–3** were determined at 113 K on a Rigaku Saturn CCD diffractometer equipped with Mo-Kα radiation (λ = 0.71073 Å), while the data for **4** was collected at 150 K on an Oxford Diffraction Gemini E system (Mo-Kα, λ = 0.71073 Å). Absorption corrections were performed through multi-scan. All structures were solved with the SHELXS-2014 structure solution program[43] and refined anisotropically by using full-matrix least-squares based on F^2 with version of SHELXL-2014.[44] All hydrogen atoms were geometrically placed. Some restraints, such as ISOR, DFIX, DELU, SADI, DANG, FLAT, RIGU and SIMU were employed on some of the disorderly C atoms and F atoms to ensure convergence of the refinement process. These data of **1-4** can be obtained freely with CCDC numbers 2142417-2142420 from The Cambridge Crystallographic Data Centre.

Synthesis of $[Ln_2Cu(hfac)_8(NITPhTzbis)_2][LnCu(hfac)_5(NITPhTzbis)]_2$

$Ln(hfac)_3{\cdot}2H_2O$ (0.01 mmol) and $Cu(hfac)_2{\cdot}2H_2O$ (0.01 mmol) were suspended in 25 mL of dry n-heptane, which was kept under refluxing for 6 hours. Then, a dichloromethane solution containing NITPhTzbis (0.01 mmol) was slowly added to the above system and the obtained solution was kept heating for another 16 minutes. The resulting mixture was filtered after cooling and placed at room temperature to allow the slow evaporation of the solvent. Block-shaped dark blue crystals suitable for X-ray diffraction were obtained within 3 days.

$[Y_2Cu(hfac)_8(NITPhTzbis)_2][YCu(hfac)_5(NITPhTzbis)]_2$ (1). Yield 61%; Elemental analysis (%) calcd for $C_{178}H_{138}Cu_3Y_4F_{108}N_{28}O_{52}$ (M_W = 6099.42): C, 35.08; H, 2.22; N, 6.43. Found: C, 35.15; H, 2.48; N, 6.55. FT-IR (cm^{-1}): 1650 (s), 1505 (m), 1350 (m), 1251 (s), 1201 (s), 1138 (s), 993 (m), 870 (m), 797 (s), 659 (s), 587 (s), 544 (m).

$[Tb_2Cu(hfac)_8(NITPhTzbis)_2][TbCu(hfac)_5(NITPhTzbis)]_2$ (2). Yield 63%; Elemental analysis (%) calcd for $C_{178}H_{134}Cu_3Tb_4F_{108}N_{28}O_{52}$ (M_W = 6375.42): C, 33.53; H, 2.12; N, 6.15. Found: C,

33.15; H, 2.48; N, 6.55. FT-IR (cm^{-1}): 1649 (s), 1503 (m), 1351 (m), 1253 (s), 1200 (s), 1140 (s), 995 (m), 869 (m), 798 (s), 660 (s), 585 (s), 545 (m).

$[Dy_2Cu(hfac)_8(NITPhTzbis)_2][DyCu(hfac)_5(NITPhTzbis)]_2$ (3). Yield 59%; Elemental analysis (%) calcd for $C_{178}H_{134}Cu_3Dy_4F_{108}N_{28}O_{52}$ (M_W = 6389.74): C, 33.46; H, 2.11; N, 6.14. Found: C, 33.75; H, 2.56; N, 6.38. FT-IR (cm^{-1}): 1650 (s), 1503 (m), 1351 (m), 1252 (s), 1202 (s), 1139 (s), 994 (m), 869 (m), 797 (s), 660 (s), 585 (s), 545 (m).

$[Ho_2Cu(hfac)_8(NITPhTzbis)_2][HoCu(hfac)_5(NITPhTzbis)]_2$ (4). Yield 61%; Elemental analysis (%) calcd for $C_{178}H_{134}Cu_3Ho_4F_{108}N_{28}O_{52}$ (M_W = 6099.42): C, 33.41; H, 2.11; N, 6.13. Found: C, 33.11; H, 2.52; N, 6.22. FT-IR (cm^{-1}): 1649 (s), 1504 (m), 1351 (m), 1252 (s), 1201 (s), 1140 (s), 995 (m), 869 (m), 798 (s), 660 (s), 586 (s), 544 (m).

Table 1. Crystallographic data and structure refinement details of complexes **1**-**4**.

Complex	**1** (CuY)	**2** (CuTb)	**3** (CuDy)	**4** (CuHo)
Formula	$C_{178}H_{134}Cu_3Ln_4F_{108}N_{28}O_{52}$			
M($g\cdot mol^{-1}$)	6095.38	6375.42	6389.74	6399.46
T(K)	113(2)	113(2)	113(2)	150(2)
Crystal system	Triclinic	Triclinic	Triclinic	Triclinic
Space group	$P\bar{1}$	$P\bar{1}$	$P\bar{1}$	$P\bar{1}$
a(Å)	14.695(3)	14.696(3)	14.789(3)	14.6422(6)
b(Å)	21.213(4)	21.242(4)	21.301(4)	21.1036(9)
c(Å)	21.502(4)	21.576(4)	21.621(4)	21.4102(8)
α(deg)	85.16(3)	85.11(3)	85.11(3)	85.124(3)
β(deg)	71.34(3)	71.23(3)	71.25(3)	71.356(4)
γ(deg)	85.75(3)	85.78(3)	85.82(3)	85.871(3)
V($Å^3$)	6320(2)	6346(2)	6419(3)	6238.9(5)
Z	1	1	1	1
D_{calcd}($g\cdot cm^{-3}$)	1.602	1.668	1.653	1.703
M(mm^{-1})	1.308	1.498	1.544	1.658
θ(deg)	1.491–25.000	1.342–25.010	1.338–25.010	2.9828–25.010
F(000)	3029	3133	3137	3141
Reflnscollected	61433	61509	51809	52184
Uniquerefln s/R_{int}	22233/0.1425	22348/0.0697	21888/0.0813	21988/0.0813
GOF(F^2)	1.060	1.059	1.066	1.040
R_1/wR_2($I>2\sigma(I)$)	0.1204/0.3026	0.0820/0.2224	0.0980/0.2488	0.0958/0.2410
R_1/wR_2(all data)	0.2169/0.3768	0.1093/0.2531	0.1266/0.2754	0.1340/0.2679

$R_1 = \Sigma(||F_o| - |F_c||)/\Sigma|F_o|$, $wR_2 = [\Sigma w(|F_o|^2 - |F_c|^2)^2/\Sigma w(|F_o|^2)^2]^{1/2}$

Results and discussion

Description of the Crystal Structures

Complexes **1–4** were characterized by single-crystal X-ray diffraction, revealing that **1–4** are all isomorphous and crystallized in the triclinic system with the $P\bar{1}$ space group. Crystallographic details and structural solutions are summarized in Table 1, and the selected bond lengths and angles are listed in Tables S1-S4. ORTEP drawing of all four structures are displayed in Figure S2.

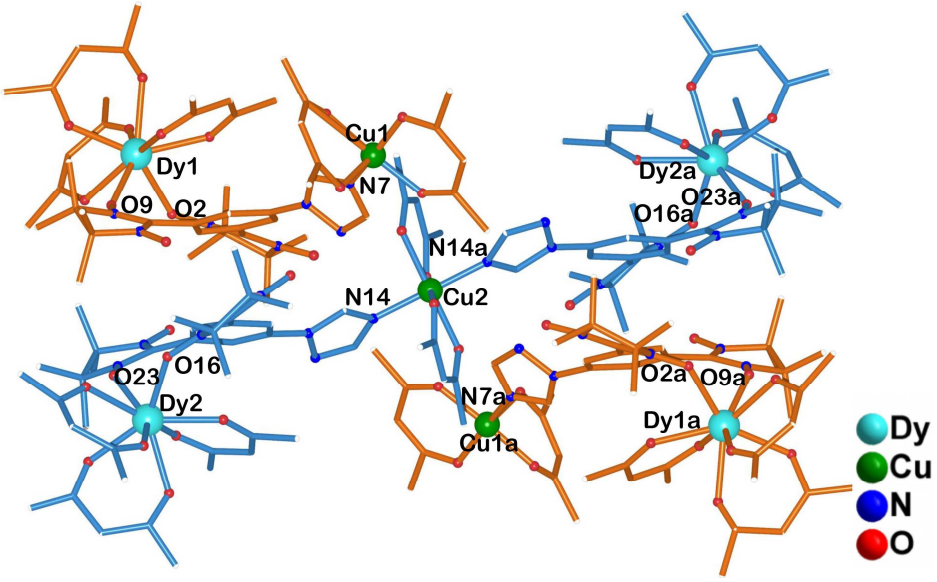

Figure 1. Heptanuclear supramolecular structure of complex **3**. Fluorine and hydrogen atoms are omitted for the sake of clarity.

For simplicity, only the structure of complex **3** will be described in detail as a representative. Complex **3** is composed of two dinuclear units [DyCu(hfac)$_5$(NITPhTzbis)] (blue in Figure 1) and one trinuclear unit [Dy$_2$Cu(hfac)$_8$(NITPhTzbis)$_2$] (orange in Figure 1). In all units, the Dy^{III} ion is coordinated by two neighboring nitroxide moieties of a NITPh-Tzbis ligand in a chelating manner and by three bidentate β-diketonate coligands (Dy1–O$_{hfac}$: 2.321(9)–2.435(9) Å), forming a coordination polyhedron with biaugmented trigonal prism (C_{2v}) geometry (Figure 2, SHAPE software,[45] Table S5). The Dy–O$_{rad}$ bond lengths (Dy–O$_{rad}$: 2.359(9)–2.414(8) Å) are consistent with those reported in other Dy(hfac)$_3$-nitronyl nitroxide biradical complexes.[46] The N–O bond lengths of a NIT unit are unequivalent, it is slightly longer for the N-O involved in coordination to a metal ion. Torsion angles of Dy–O–N–C are 60.8(16)°, 65.4(15)° for Dy1 in dinuclear unit and 57.0(17)°, 62.0(17)° for Dy2 in trinuclear unit. The dihedral angles formed between the radical ON–C–NO plane and the benzene ring are 26.7(6)°, 25.0(5)° for dinuclear unit and 31.2(7)°,

28.0(3)° for trinuclear unit, while dihedral angles formed by the triazole ring and the benzene ring are 46.6(3)° and 28.5(4)°, respectively.

Two different types of Cu^{II} ions are found co-exist within the structure. The Cu1 center in dinuclear unit is five-coordinated, with one N atom from the triazole unit and four O atoms from two *β*-diketonate coligands. The coordination sphere exhibits a distorted pyramidal geometry. As a result of *Jahn-Teller* effect, one O atom of a *β*-diketonate coligand is located in the apical position, showing a significantly longer bond length (Cu1-O:2.219(9) Å) than those atoms in equatorial positions (Cu1-N: 1.988(9) Å; Cu1-O: 1.936(9)-1.972(9) Å). The Cu^{II}-Dy^{III} distance through phenyl and triazole rings in dinuclear is 10.312 Å.

The Cu2 center in trinuclear unit sits in a distorted octahedron. The equatorial positions are occupied by two N atoms which come from the triazole moieties of two biradicals (Cu2-N: 1.990(9) Å) and two O atoms of *β*-diketonate coligands (Cu2-O: 2.083(9) Å). These coligands also provide another two O atoms coordinated to the Cu2 center in the apical positions with longer bond length (Cu2-O: 2.201(9) Å), which indicates a *Jahn-Teller* effect. The Cu^{II}-Dy^{III} distance through phenyl and triazole rings in trinuclear is 10.571 Å. Furthermore, the different coordination spheres of two kinds of Cu^{II} centers may be responsible for the relatively large differences in dihedral angles formed by triazole rings and benzene rings.

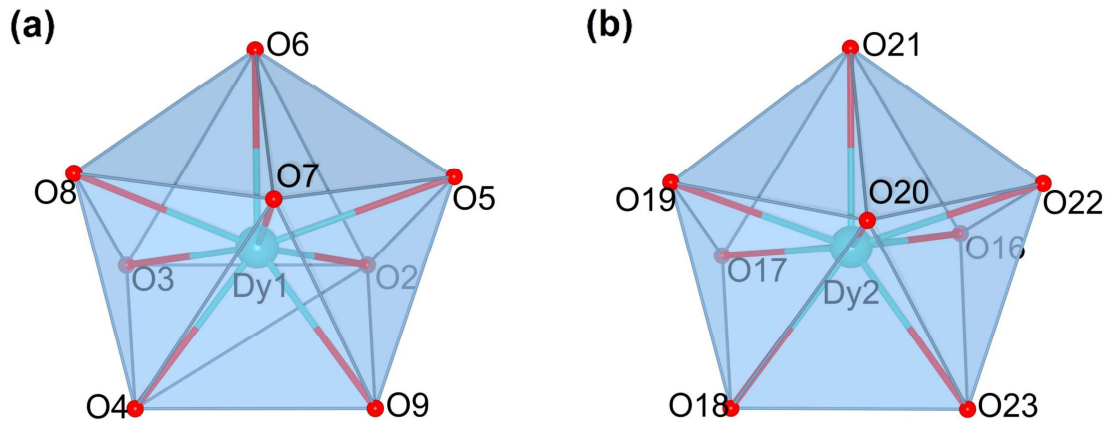

Figure 2. Coordination polyhedron of Dy^{III} ions in (a) dinuclear and (b) trinuclear unit respectively.

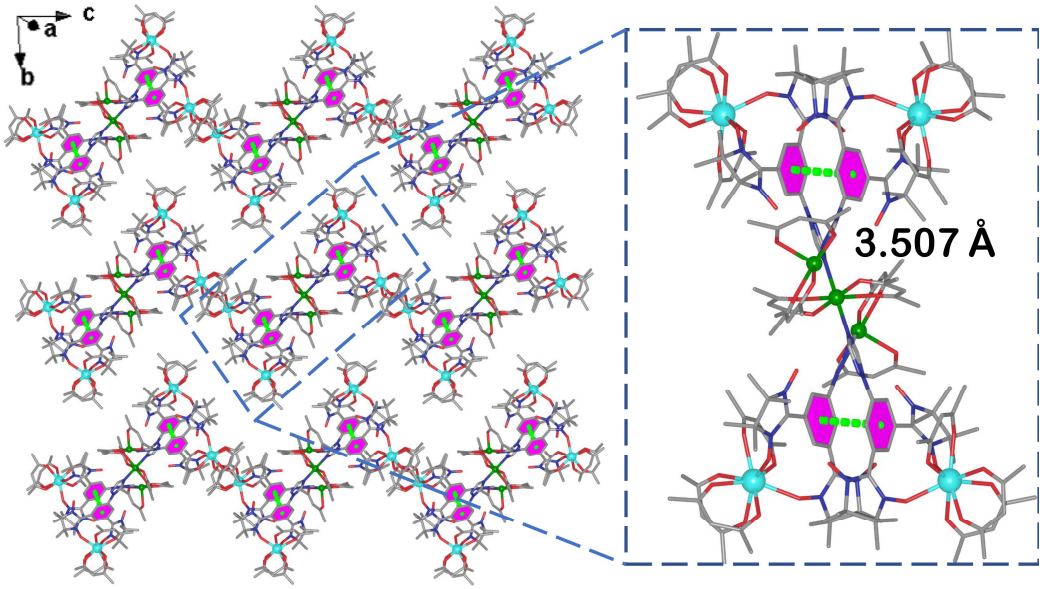

Figure 3. Packing arrangement formed by π–π interaction in DyCu complex.

The dinuclear and trinuclear units are gripped together through the π–π interactions between the benzene rings of NITPhTzbis ligans(distance 3.507 Å, Figure 3) to form the heptanuclear supermolecule. In the heptanuclear cluster of **3**, the Dy1···Dy2, Dy1···Dy2a and Dy1···Dy1a distances are 9.823 Å, 18.328 Å, and 20.373 Å, respectively, and the distance between Cu1 and Cu2 is 7.741 Å. The shortest separation between the uncoordinated N–O groups is 4.043 Å. It should be noted that, for this supramolecule structure, there are short distances between radical moieties involving the uncoordinated NO group and the sp^2 carbon atoms of NIT (O24---C7: 3.776 Å; O10---C54: 3.135 Å) as revealed in Figure S3. The views of the crystal packing of all complexes are shown in Figure 3 and Figure S4.

Magnetic studies. The temperature-dependent molar magnetic susceptibility (χ_M) of complexes **1–4** were collected between 2 and 300 K under a dc field of 1000 Oe (Figure 4). The values of $\chi_M T$ product at 300 K for complexes **1–4** are 4.46, 52.00, 61.70 and 60.97 $cm^3 \cdot K \cdot mol^{-1}$, respectively, which are close to the Curie contributions (4.13 $cm^3 \cdot mol^{-1}$ K for **1**, 51.41 $cm^3 \cdot mol^{-1}$ K for **2**, 60.81 $cm^3 \cdot mol^{-1}$ K for **3** and 60.41 $cm^3 \cdot mol^{-1}$ K for **4**) expected for four Ln^{III} ions, three Cu^{II} ions (S = 1/2) and eight S = 1/2 radicals in the absence of magnetic exchange interactions. For YCu complex, the $\chi_M T$ value gradually increased, reaching the maximum value of 6.56 $cm^3 mol^{-1} K$ at 2 K, indicating a significant ferromagnetic coupling effect. The field dependence of the molar magnetization (M) for **1** was measured at 2–5 K in the field range of 0–50 kOe (Figure

4a inset). For the *M-H* curve at 2.0 K, it shows a sustained rise to reach to 10.18 Nβ at 50 kOe, which is basically consistent with theoretical saturation value of 11 Nβ.

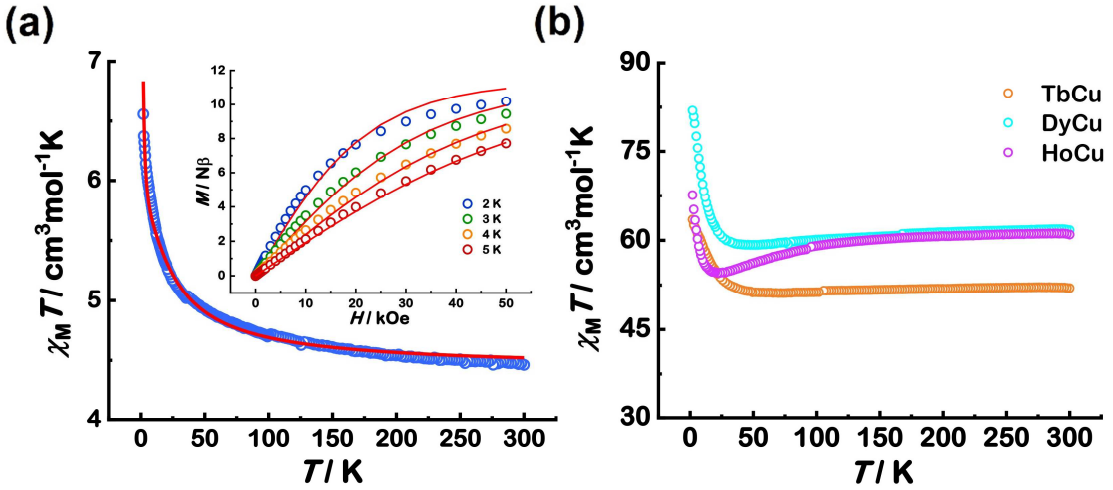

Figure 4. (a) $\chi_M T$ vs. T curve for the YCu analogue, inset shows M vs. H curves in the field range 0–50 kOe and at the temperature range of 2–5 K (the solid line represents best fitted behavior by PHI). (b) $\chi_M T$ vs. T curves for TbCu, DyCu and HoCu analogues.

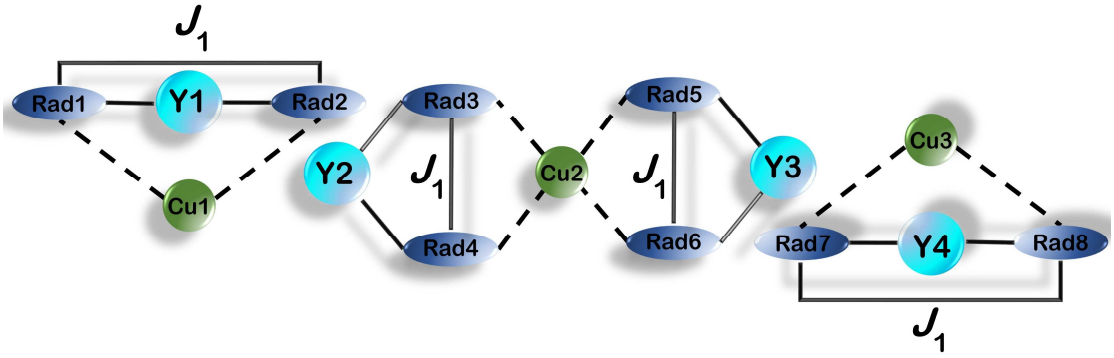

Scheme 2. Magnetic exchange interactions in **1.**

According to the crystal structure of **1**, two kinds of magnetic exchanges might be anticipated. One is the interaction between the two aminoxyl units belonging to the same ligand (J_1, in Scheme 2*)* and this interaction may take place through Y^{III} and/or the m-phenylene ring; the second is the magnetic interaction between the radicals and a Cu^{II} ion transmitted through the benzene ring and the triazole ring. However, latter should be so weak that it can be ignored. Therefore, the magnetic behavior of **1** is best described as four [rad-Y-rad] units plus three isolated Cu^{II} ions (Scheme 2). To account for possible weak interactions within or between binuclear and trinuclear units, a mean-field parameter zJ' was introduced. Modeling was performed with PHI software,[47] results are given based on the following Hamiltonian:

$$\hat{H} = -2J_1\left(\hat{S}_{rad1}\hat{S}_{rad2}\right)$$

The simultaneous fitting of $\chi_M T$ versus T and magnetization data (Figure 4a) for **1** resulted in J_1 = 12.49 cm^{-1}, zJ'= 0.020 cm^{-1}, g_{Cu} = 2.25, g_{rad} = 2.00 (fixed). The positive value of J_1 indicates that a ferromagnetic NIT---NIT exchange dominates in the system, which is in line with the reported results.[48, 49] This ferromagnetic contribution can be attributed to the magnetic coupling between two NIT via *m*-phenylene ring that is anticipated to be ferromagnetic based on spin polarization,[33] whereas the magnetic exchange between two NO units through Y ion has been reported to be weakly antiferromagnetic.[50,51] The small positive zJ' indicates a weak intermolecular ferromagnetic coupling likely resulting from through-space interactions between closely spaced radicals. Indeed, the opposite spin polarization between the oxygen atom of the NO group in NITPhTzbis and the sp^2 carbon atom of the adjacent NITPhTzbis (Figure 5) should lead to ferromagnetism according to the McConnells mechanism.[52, 53]

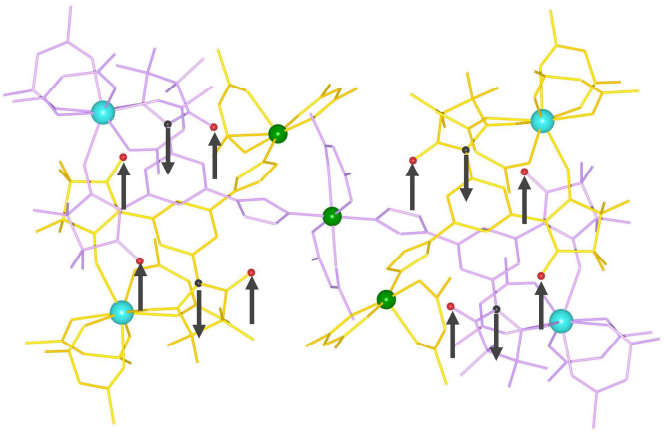

Figure 5. Spin interactions responsible for the ferromagnetic coupling based on McConnells mechanism.

For complexes **2** and **3**, the $\chi_M T$ value shows a slight diminution as the temperature down to about 70 K for **2** and 50K for **3**, followed by a rapid increase in the lower temperature domain and reaches the maximum value of 63.47 $cm^3 \cdot mol^{-1}$ K for **2** and 81.91 $cm^3 \cdot mol^{-1}$ K for **3**. For **4**, the $\chi_M T$ value first gradually decreases to 54.54 $cm^3 \cdot mol^{-1}$ K and then increase quickly to 67.61 $cm^3 \cdot mol^{-1}$ K at 2 K. For these three complexes, the decrease of $\chi_M T$ curve at high temperature mainly results from thermal depopulation of the Stark sublevels (i.e. the crystal field effect) of the Ln^{III} ions, while the increases at low temperature region may results from the ferromagnetic interactions in the [NIT-Ln-NIT] units.[54, 55]

The molar magnetizations (*M*) of **2–4** were also measured 2.0–5.0 K with external fields(*H*) in the range of 0–50 kOe (Figure S5). At 2.0K, for three complexes, the intensity of magnetization increased steeply as the field increased to 10 kOe, then follow a gradual increase till reaching 28.94, 29.64 and 30.81Nβ at 50 kOe for **2**-**4**, respectively. Besides, *M*(*H*/*T*) curves of **2–4** were not superimpose completely, suggesting the presence of significant magnetic anisotropy.[56]

Dynamic Susceptibility Studies.

Alternating-current (ac) magnetic susceptibility measurements were performed for complexes **2–4** in zero dc field between 2 and 20 K to examine the spin dynamics. For **3**, out-of phase signals (*χ"*) appeared (Figure S6), indicating a possible slow magnetic relaxation behavior, however, no peaks for *χ"* were observed above 2 K, likely due to quantum tunnelling of magnetization (QTM). When a static field was applied (400 Oe was found to be the optimal field, see Figure S7), QTM was suppressed effectively and both frequency and temperature-dependent out-of-phase (*χ"*) peaks were observed (Figure 6), evidencing slow magnetic relaxation behaviour for DyCu complex **3**.

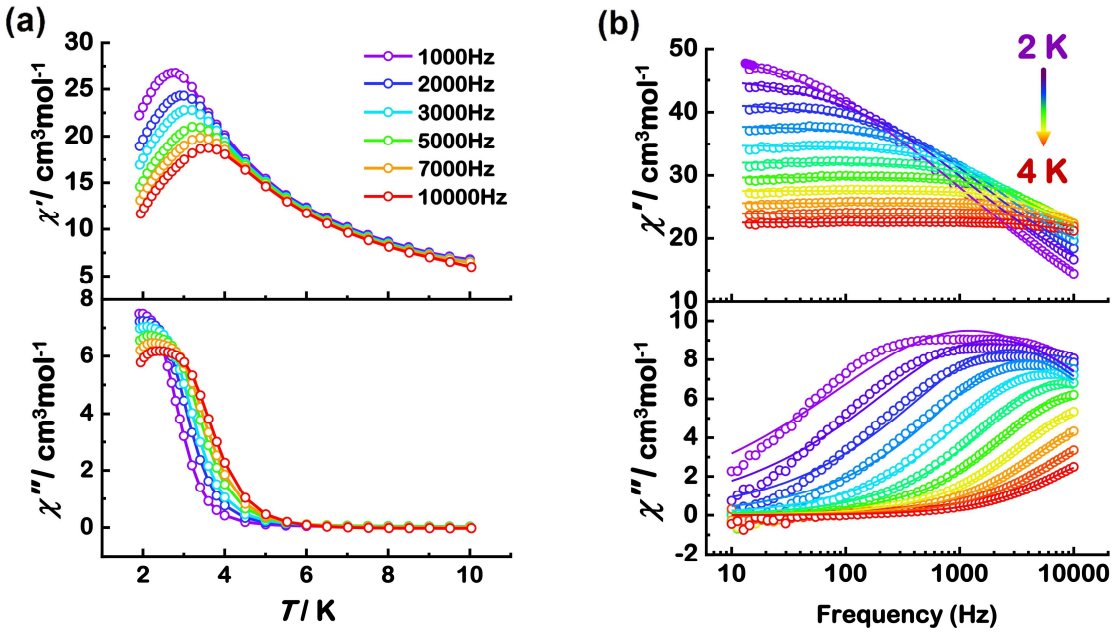

Figure 6. Temperature (left) and frequency dependence (right) of the in-phase and out-of-phase ac susceptibilities under applied dc field of 400 Oe for complex **3**.

Further insight in the relaxation dynamics of **3** was obtained by extracting relaxation times (*τ*) from *χ"*(*ν*) data using the generalized Debye model.[57, 58] The analysis of the temperature

dependence of τ with the Arrhenius equation $\tau = \tau_0 \, exp \, (U_{eff}/k_BT)$ gave the energy barrier for the reversal of the magnetization U_{eff} of 10.8 K with the pre-exponential factor $\tau_0 = 6.3 \times 10^{-7}$ s (Figure 7a). Furthermore, the Cole-Cole diagrams of **3** (Figure 7b) were also constructed and fitted by using a generalized Debye model and the obtained α values are in the range of 0.06-0.55, indicating a moderate distribution of relaxation time. For complex **2,** only the onset of a weak out-of-phase signal was observed whether in zero field or with applied field (Figure S8a) while, for compound **4,** no out-of-phase signal was observed (Figure S8b).

It is appealing to compare complex **3** with related biradical-based Dy complexes. By reviewing complexes with related isolated [NIT-Dy-NIT] tri-spin fragment (Table S6)[46, 59-61], those nitronyl nitroxide biradical Dy complexes exhibit magnetic relaxation behavior except for a MnDy complex[59] in which the local symmetry of the Dy ion belongs to D_{2d}. This means that the symmetry of the local crystal-field of Dy ion play crucial role on the magnetic relaxation. For these complexes, including **3**, the values of effective energy barriers show some differences and this could be attributed to slightly different exchange interactions, the local symmetry of the Ln ion and supramolcular interactions.

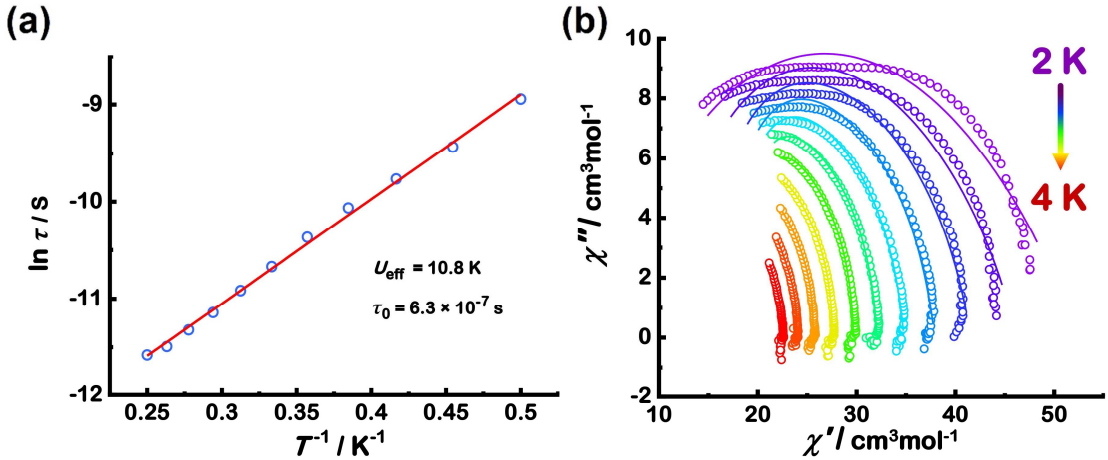

Figure 7. Plot of lnτ versus T^{-1} (a) and Cole-Cole diagrams at different temperatures under a 400 Oe dc field (b) for **3** (the solid line stands for the fitting results).

Conclusion

Using a novel nitronyl nitroxide biradical functionalized by a triazole group (NITPhTzbis), four biradical–Ln–Cu complexes have been obtained. In these complexes, consist in a heptanuclear supramolecular structure formed dinuclear [$LnCu(hfac)_5$(NITPhTzbis)] and trinuclear [$Ln_2Cu(hfac)_8$($NITPhTzbis)_2$] units assembled through π---π interactions. Their magnetic

behaviors are governed by intramolecular Ln-NO (Ln = Tb, Dy, Ho) and intermolecular ferromagnetic interactions. Interestingly, CuDy derivative shows magnetic relaxation behavior. This work demonstrates that functional nitronyl nitroxide biradicals are appealing building blocks to construct SMMs with lanthanides and their magnetic properties could be tuned by different functional substituents via ligating transition metal ions.

Conflicts of interest

There are no conflicts of interest to declare.

Author contributions

Lu Xi: investigation, fitting the magnetic data; writing - original draft; **Chao-Yi Jin:** investigation; **Hong-Wei Song:** data analysis; **Xiao-Tong Wang:** data analysis; **Licun Li**: Supervision, Writing - review and editing, Funding acquisition; **Jean-Pascal Sutter:** Magnetic measurements, Writing - review and editing. All authors have given approval to the final version of the manuscript.

Acknowledgements

This work was financially supported by the National Key R&D Program of China (2018YFA0306002) and the National Natural Science Foundation of China (No. 21773122).

References

1. N. Ishikawa, M. Sugita, T. Ishikawa, S.-y. Koshihara and Y. Kaizu, *J. Am. Chem. Soc.*, 2003, **125**, 8694-8695.
2. P. Zhang, L. Zhang, C. Wang, S. Xue, S.-Y. Lin and J. Tang, *J. Am. Chem. Soc.*, 2014, **136**, 4484-4487.
3. Y. Chen, F. Ma, X. Chen, B. Dong, K. Wang, S. Jiang, C. Wang, X. Chen, D. Qi, H. Sun, B. Wang, S. Gao and J. Jiang, *Inorg. Chem.*, 2017, **56**, 13889-13896.
4. J. L. Liu, Y. C. Chen and M. L. Tong, *Chem. Soc. Rev.*, 2018, **47**, 2431-2453.
5. F.-S. Guo, A. K. Bar and R. A. Layfield, *Chem. Rev.*, 2019, **119**, 8479-8505.
6. C. A. P. Goodwin, F. Ortu, D. Reta, N. F. Chilton and D. P. Mills, *Nature*, 2017, **548**, 439-442.
7. F.-S. Guo, B. M. Day, Y.-C. Chen, M.-L. Tong, A. Mansikkamäki and R. A. Layfield, *Angew. Chem. Int. Ed.*, 2017, **56**, 11445-11449.
8. Y.-S. Ding, N. F. Chilton, R. E. P. Winpenny and Y.-Z. Zheng, *Angew. Chem. Int. Ed.*, 2016, **55**, 16071-16074.
9. J. Liu, Y.-C. Chen, J.-L. Liu, V. Vieru, L. Ungur, J.-H. Jia, L. F. Chibotaru, Y. Lan, W. Wernsdorfer, S. Gao, X.-M. Chen and M.-L. Tong, *J. Am. Chem. Soc.*, 2016, **138**, 5441-5450.
10. F.-S. Guo, B. M. Day, Y.-C. Chen, M.-L. Tong, A. Mansikkamäki and R. A. Layfield, *Science*, 2018, **362**, 1400.
11. Y.-N. Guo, G.-F. Xu, W. Wernsdorfer, L. Ungur, Y. Guo, J. Tang, H.-J. Zhang, L. F. Chibotaru and A. K. Powell, *J. Am. Chem. Soc.*, 2011, **133**, 11948-11951.
12. J. Long, F. Habib, P. H. Lin, I. Korobkov, G. Enright, L. Ungur, W. Wernsdorfer, L. F. Chibotaru and M. Murugesu, *J. Am. Chem. Soc.*, 2011, **133**, 5319-5328.
13. T. Pugh, N. F. Chilton and R. A. Layfield, *Angew. Chem. Int. Ed.*, 2016, **55**, 11082-11085.
14. Y. Horii, K. Katoh, B. K. Breedlove and M. Yamashita, *Chem. Commun.*, 2017, **53**, 8561-8564.
15. F. Habib, J. Long, P.-H. Lin, I. Korobkov, L. Ungur, W. Wernsdorfer, L. F. Chibotaru and M. Murugesu, *Chem. Sci*, 2012, **3**.
16. T. Fukuda, K. Matsumura and N. Ishikawa, *J. Phys. Chem. A*, 2013, **117**, 10447-10454.
17. S. Dhers, J.-P. Costes, P. Guionneau, C. Paulsen, L. Vendier and J.-P. Sutter, *Chem. Commun.*, 2015, **51**, 7875-7878.
18. S. Demir, I.-R. Jeon, J. R. Long and T. D. Harris, *Coord. Chem. Rev.*, 2015, **289–290**, 149-176.
19. J. D. Rinehart, M. Fang, W. J. Evans and J. R. Long, *J. Am. Chem. Soc.*, 2011, **133**, 14236-14239.
20. N. Mavragani, D. Errulat, D. A. Gálico, A. A. Kitos, A. Mansikkamäki and M. Murugesu, *Angew. Chem. Int. Ed.*, 2021, **60**, 24206-24213.
21. F. Liu, L. Spree, D. S. Krylov, G. Velkos, S. M. Avdoshenko and A. A. Popov, *Acc. Chem. Res.*, 2019, **52**, 2981-2993.
22. F. Liu, G. Velkos, D. S. Krylov, L. Spree, M. Zalibera, R. Ray, N. A. Samoylova, C.-H. Chen, M. Rosenkranz, S. Schiemenz, F. Ziegs, K. Nenkov, A. Kostanyan, T. Greber, A. U. B. Wolter, M. Richter, B. Büchner, S. M. Avdoshenko and A. A. Popov, *Nat. Commun.*, 2019, **10**, 571.
23. D. Amabilino, J. Vaciana, M. Miller and M. Drillon, *Magnetism: Molecules to Materials II: Molecule-Based Materials*, 2002.
24. D. Luneau and P. Rey, *Coord. Chem. Rev.*, 2005, **249**, 2591-2611.
25. A. Caneschi, D. Gatteschi, N. Lalioti, C. Sangregorio, R. Sessoli, G. Venturi, A. Vindigni, A. Rettori, M. G. Pini and M. A. Novak, *Angew. Chem. Int. Ed.*, 2001, **40**, 1760-1763.

26. R. A. A. Cassaro, S. G. Reis, T. S. Araujo, P. M. Lahti, M. A. Novak and M. G. F. Vaz, *Inorg. Chem.*, 2015, **54**, 9381-9383.
27. M. G. F. Vaz, R. A. A. Cassaro, H. Akpinar, J. A. Schlueter, P. M. Lahti and M. A. Novak, *Chem. Eur. J*, 2014, **20**, 5460-5467.
28. I. A. Gass, S. Tewary, A. Nafady, N. F. Chilton, C. J. Gartshore, M. Asadi, D. W. Lupton, B. Moubaraki, A. M. Bond, J. F. Boas, S.-X. Guo, G. Rajaraman and K. S. Murray, *Inorg. Chem.*, 2013, **52**, 7557-7572.
29. L. M. Field, M. C. Morón, P. M. Lahti, F. Palacio, A. Paduan-Filho and N. F. Oliveira, *Inorg. Chem.*, 2006, **45**, 2562-2567.
30. K. Hamachi, K. Matsuda, T. Itoh and H. Iwamura, *Bull. Chem. Soc. Jpn.*, 1998, **71**, 2937-2943.
31. E. Tretyakov, S. Fokin, G. Romanenko, V. Ikorskii, S. Vasilevsky and V. Ovcharenko, *Inorg. Chem.*, 2006, **45**, 3671-3678.
32. A. Caneschi, P. Chiesi, L. David, F. Ferraro, D. Gatteschi and R. Sessoli, *Inorg. Chem.*, 1993, **32**, 1445-1453.
33. L. Catala, J. Le Moigne, N. Kyritsakas, P. Rey, J. J. Novoa and P. Turek, *Chem. Eur. J*, 2001, **7**, 2466-2480.
34. M. Zhu, X. Mei, Y. Ma, L. Li, D. Liao and J.-P. Sutter, *Chem. Commun.*, 2014, **50**, 1906-1908.
35. X. Wang, P. Hu, L. Li and J.-P. Sutter, *Inorg. Chem.*, 2015, **54**, 9664-9669.
36. M. Zhu, L. Li and J.-P. Sutter, *Inorganic Chemistry Frontiers*, 2016, **3**, 994-1003.
37. A. A. Patrascu, M. Briganti, S. Soriano, S. Calancea, R. A. Allão Cassaro, F. Totti, M. G. F. Vaz and M. Andruh, *Inorg. Chem.*, 2019, **58**, 13090-13101.
38. A. A. Patrascu, S. Calancea, M. Briganti, S. Soriano, A. M. Madalan, R. A. A. Cassaro, A. Caneschi, F. Totti, M. G. F. Vaz and M. Andruh, *Chem. Commun.*, 2017, **53**, 6504-6507.
39. M. G. F. Vaz and M. Andruh, *Coord. Chem. Rev.*, 2021, **427**, 213611.
40. E. F. Ullman, L. Call and J. H. Osiecki, *J. Org. Chem.*, 1970, **35**, 3623-3631.
41. E. F. Ullman, J. H. Osiecki, D. G. B. Boocock and R. Darcy, *J. Am. Chem. Soc.*, 1972, **94**, 7049-7059.
42. E. A. Boudreaux and L. N. Mulay, *Theory and applications of molecular paramagnetism*, Wiley-Interscience, New York, 1976.
43. G. M. Sheldrick, *SHELXS-2014, Program for structure solution*, Universität of Göttingen, Göttingen, Germany, 2014.
44. G. M. Sheldrick, *SHELXL-2014, Program for structure refinement*, Universität of Göttingen, Göttingen, Germany, 2014.
45. D. Casanova, M. Llunell, P. Alemany and S. Alvarez, 2005, **11**, 1479-1494.
46. K. Bernot, F. Pointillart, P. Rosa, M. Etienne, R. Sessoli and D. Gatteschi, *Chem. Commun.*, 2010, **46**, 6458-6460.
47. J. O. Moilanen, N. F. Chilton, B. M. Day, T. Pugh and R. A. Layfield, *Angew. Chem. Int. Ed.*, 2016, **55**, 5521-5525.
48. L. Xi, H. Li, J. Sun, Y. Ma, J. Tang and L. Li, *Inorg. Chem.*, 2020, **59**, 443-451.
49. J. Xie, H.-D. Li, M. Yang, J. Sun, L.-C. Li and J.-P. Sutter, *Chem. Commun.*, 2019, **55**, 3398-3401.
50. C. Benelli, A. Caneschi, D. Gatteschi, L. Pardi and P. Rey, *Inorg. Chem.*, 1989, **28**, 3230-3234.
51. J.-P. Sutter, M. L. Kahn, S. Golhen, L. Ouahab and O. Kahn, *Chem. Eur. J*, 1998, **4**, 571-576.
52. H. M. McConnell, *J. Chem. Phys*, 1963, **39**, 1910-1910.
53. F. Lanfranc de Panthou, D. Luneau, J. Laugier and P. Rey, *J. Am. Chem. Soc.*, 1993, **115**, 9095-9100.
54. M. L. Kahn, J.-P. Sutter, S. Golhen, P. Guionneau, L. Ouahab, O. Kahn and D. Chasseau, *J. Am. Chem. Soc.*, 2000, **122**, 3413-3421.
55. J.-P. Sutter, M. L. Kahn and O. Kahn, *Adv. Mater.*, 1999, **11**, 863-865.
56. D. I. Alexandropoulos, L. Cunha-Silva, L. Pham, V. Bekiari, G. Christou and T. C. Stamatatos, *Inorg. Chem.*,

2014, **53**, 3220–3229.

57. K. S. Cole and R. H. Cole, *J. Chem. Phys*, 1941, **9**, 341-351.
58. S. M. J. Aubin, Z. Sun, L. Pardi, J. Krzystek, K. Folting, L.-C. Brunel, A. L. Rheingold, G. Christou and D. N. Hendrickson, *Inorg. Chem.*, 1999, **38**, 5329-5340.
59. P. Jing, L. Xi, J. Lu, J. Han, X. Huang, C. Jin, J. Xie and L. Li, *Chem. Asian. J*, 2021, **16**, 793-800.
60. L. Xi, J. Sun, K. Wang, J. Lu, P. Jing and L. Li, *Dalton. Trans.*, 2020, **49**, 1089-1096.
61. K. Wang, J. Sun, L. Xi, J. Lu, P. Jing and L. Li, *Dalton. Trans.*, 2019, **48**, 14383-14389.